Ageev, E.; Andreeva, Y.; Ionin, A.; Kashaev, N.; Kudryashov, S.; Nikonorov, N.; Nuryev, R.; Petrov, A.; Rudenko, A.; Samokhvalov, A.; Saraeva, I.; Veiko, V.:

Single-shot femtosecond laser processing of Al-alloy surface: An interplay between Mbar shock waves, enhanced microhardness, residual stresses, and chemical modification.

In: Optics and Laser Technology. Vol. 126 (2020) 106131.

First published online by Elsevier: 14.02.2020

https://dx.doi.org/10.1016/j.optlastec.2020.106131

Single-shot femtosecond laser-induced peening of Al-alloy surface: interplay between Mbar shock waves, enhanced microhardness, residual stresses and chemical modification

E.I. Ageev,[1] Y.M. Andreeva,[1] A.A. Ionin,[2] N.S. Kashaev,[3] S.I. Kudryashov,[1,2] N.V. Nikonorov,[1] R.K. Nuryev,[1] A.A. Petrov,[1] A.A. Rudenko,[2] A.A. Samokhvalov,[1] I.N. Saraeva,[2] V.P. Veiko[1]

[1] ITMO University, Kronverkskiy prospect 49, 197101 St. Petersburg, Russia

[2] P.N. Lebedev Physical Institute, Leninsky prospect 53, 119991 Moscow, Russia

[3] Helmholtz-Zentrum Geesthacht, Institute of Materials Research, Materials Mechanics, Max-Planck-Str. 1, 21502 Geesthacht, Germany

Abstract: Ambient-air single-shot ablative femtosecond laser surface peening of an advanced Al-alloy AA5083for ship building was comprehensively characterized by non-contact broadband ultrasonics, scanning electron microscopy with energy-dispersion x-ray spectroscopy, x-ray diffraction and Vickers microhardness tests. The characterization indicates that the generated Mbar-level shock waves induce not only strong structural perturbation of the peened micron-thick surface layer with sub-GPa-level residual compressive and tensile stresses, rising its microhardness by almost 50%, but also significant depth-dependent chemical modification within the layer.

Key words: femtosecond laser, Al alloy AA5083, single-shot laser ablation, peening, ultrasonic diagnostics, Vickers microhardness, x-ray diffraction, energy-dispersive x-ray spectroscopy

1. Introduction

Processing of material surfaces and interfaces by ultrashort (femtosecond, fs) laser pulses has proved its ultimate precision [1], multi-scale surface relief [2] and sub-surface crystalline nanotexturing opportunities [3], as compared to "softer", presumably thermal action of short (nanosecond, ns) laser pulses [4]. Much faster fs-laser energy deposition on material surfaces results in significant mechanical influence, becoming unprecedently strong under ablation conditions via Mbar-level shock waves (SW) [5-11] and supporting a number of promising applications as surface peening, forming and enhancement of corrosion resistance [12-15]. Fs-laser driven SWs provide much higher pressures P ~10^2-10^3 GPa [5-11] versus ~1-10 GPa for ns-laser induced SWs in a water confinement regime [16], with their shock-loading times τ are by the order of magnitude comparable during fs-laser ablation [11] and water-confined ablative ns-laser plasma formation [16]. Meanwhile, typical mJ-energies of fs-laser pulses deposited into materials are much lower, than multi-J energies of industrial ns-lasers, thus yielding in smaller SW-sources and shorter-range SW-affected depths L ~10-10^2 μm for fs-laser pulses [11], as compared to water-confined ns-laser ablative SW-affected depths L ~1 mm [17]. Hence, fs-laser driven SWs were claimed to be highly efficient for WC-free *bulk* mechanical processing of *microparts or micro-devices* [17], or for ultimate *surface* processing of any materials to improve their fatigue and corrosion resistance, tribological characteristics [12-15], or for driving high-pressure solid-phase transitions [6,9].

However, common quantitative characterization of *front-side* peak pressures of fs-laser driven SWs by means of standard *rear-side* non-contact optical interferometric (see, e.g., the review [18]) or contact ultrasonic [7-8,11] methods, which is required for controllable SW-mediated fs-laser surface and interface processing, is not accurate because of non-linear short-range, pressure-dependent SW dissipation in solids over sub- and micrometer-long distances [10]. In contrast, *front-side* optical diagnostics of opaque, highly scattering micro-heterogeneous fs-laser ablative plumes and related air shock waves is possible only by side-view shadowgraphy [19] or by common front-view interferometry at very high laser fluences (~10-10^2 J/cm^2) [5], when such plumes become partially reflective owing to their considerable ionization.

Our novel strategy in SW-mediated fs-laser processing of material surface relies upon a versatile ultrasonic technique for front-side remote pressure characterization of ablative plumes and related shock waves in air [7,8,11], which is free from submicrometer-scale solid-state dissipation of strong pressure waves [10] and covers the pressure gap for intermediate fluences ~0.1-10 J/cm^2 commonly used for a wide range of surface-based technological applications [12-15]. Meanwhile, comparing to these previous SW-mediated fs-laser surface modification studies under unspecified pressurization conditions [12-15], we employ this technique to rely directly Mbar-level recoil pressures, driving super-strong peening SWs on a surface of important for ship building Al-alloy AA5083 during its ablation at variable high fs-laser fluences, and consequent structural, chemical and mechanical changes in the surface layer, characterized by comprehensive x-ray diffraction (XRD) investigation of buried residual stresses, Vickers microhardness and chemical EDX micro-analysis of the peened surface.

2. Materials and methods

Single-shot ablation of fresh spots of a Al-alloy sample was provided by linearly-polarized femtosecond laser pulses from a laser system, comprised by a Ti:sapphire oscillator TiF-100-F4 and a regenerative amplifier RAP1500 (Avesta Project Ltd.), with the central wavelength of 800 nm, half-maximum pulsewidth ≈ 100 fs, maximal pulse energy of 1.2 mJ (TEM_{00}-mode), coming at the 10-Hz repetition rate [8,11]. *S*-polarized laser pulses were focused onto the sample surface at an angle of 45^0 by a spherical silica lens (BK-7, f = 40 mm) into an elliptic spot with its main 1/e-radii $R_{1/e,x(y)} \approx 45$ and 60 μm. Laser pulse energy was reduced prior the focusing lens by a binary difraction attenuator DVA-8-800 (Avesta Project Ltd.) over the range of 0.008-0.9 mJ, providing the peak fluences F_0 up to 8 J/cm^2 in the sub-filamentation regime.

Experimental samples of 1cm×1cm wide and 0.4-mm thick mechanically-polished (RMS roughness ≈0.1 μm) plates of Al-alloy grade AA5083 (chemical composition: Al – ≈94%, Mg – ≈4.4%, Mn ≈ ≤1%, other elements – Fe, Si, Zn, Cu, Cr, Ti < 0.4%) were arranged onto a two-dimensional motorized translation stage 8MT175 (Standa) and translated from laser shot to shot to warrant their single-shot exposures during ultrasonic studies and surface peening processing. Scanning electron microscopy (SEM) and energy-dispersion X-ray fluorescence spectroscopy (EDX) characterization of surface topographies and chemical composition of the ablated surfaces was performed using a JEOL 7001F microscope and related Inca Energy X-Max module (Oxford Instruments), respectively, while their preliminary optical

inspection was provided by an optical microscope Axio Imager A1.m (Carl Zeiss). X-ray diffraction studies were performed in the angle range 2θ =25-100° by means of a diffractometer Rigaku Ultima IV at the wavelength $\lambda_{(Cu\text{-}K\alpha)}$ = 1.5418 Å, using the Bragg-Brentano geometry.

Mechanical behavior of laser-peened and original (reference) surface was tested using a square-based Vickers diamond pyramid as an indenter to perform static microhardness measurements with a standard PMT-3M (LOMO, Russia) microhardness tester. The indention tests were conducted in air with 50-g indenter load during 10 s over 10 different points across the samples. To ensure an accurate measurement of diagonal lengths of imprints for the indenter, the high-resolution optical microscope Axio Imager A1.m (Carl Zeiss, Germany) was used. Typical diagonal lengths of the imprints were ≈ 20 μm, while their depths approached to 6-7 μm [20], being comparable to single-shot fs-laser peened depths ~ 3-7 μm [11] and thus providing rather adequate in-depth hardness probing.

During our non-contact ultrasonic measurements, a broad-band piezo-electric transducer MiniWAT-2 (20-μm thick PVDF-film as an active piezoelement, protected by a frontal 30-μm thick aluminum foil electrode and supported by a 10-mm thick epoxy glue layer, effective bandwidth with a pre-amplifier ≤ 30 MHz, sensitivity – 10 V/bar) [7] was arranged at the fixed distance L_{TR} =5.2±0.1 mm along the normal to the sample surface in front of the focal spot (Fig.1). The focal spot dimensions and the transit distance dictated the far-field ultrasonic acquisition zone with the corresponding differentiated, almost symmetrical bipolar transients of the unipolar ablative pressure pulses [7] (Fig.1, inset). The first bipolar electrical pulse with its delay (T_{TR}) and FWHM (T_W) times and amplitude P_{TR} from the transducer was acquired, using a 50-Om input of a digital oscilloscope TDS-3032C (Tektronix), triggered by a pulse from a laser-fed fast photodiode DET-210 (Thorlabs, response time ≈1 ns). The fluence dependence of the ultrasonic transit time, $T_{TR}(F_0)$, was used to evaluate initial fluence-dependent ablative pressures P_{ABL}, driving in air the acquired shock waves, by means of the numerical code PEFS-2 [7,8,11]. Specifically, each measured value T_{TR} was considered as a sum of a supersonic propagation time period T_1 during the first, point-explosion stage with its pressure, dropping radially and temporally as $\propto 1/R(t)^3$ [21], and of a consequent sonic propagation time period T_2, starting, when the corresponding point-explosion speed drops down to the sonic one and its frontal pressure drops as $\propto 1/R(t)$ down to the transition value ≈ 0.6 MPa [7,21]. For the fixed total transit distance L_{TR} ≈ 5 mm each longer "supersonic" time T_1 means shorter corresponding "sonic" time and overall time T_{TR}, with the initial supersonic propagation stage limited by the initial point-explosion (ablation) pressure P_{ABL} [21]. As a result, certain ablative pressure P_{ABL} can be derived (Fig.2) for each fluence-dependent transit time magnitude T_{TR}.

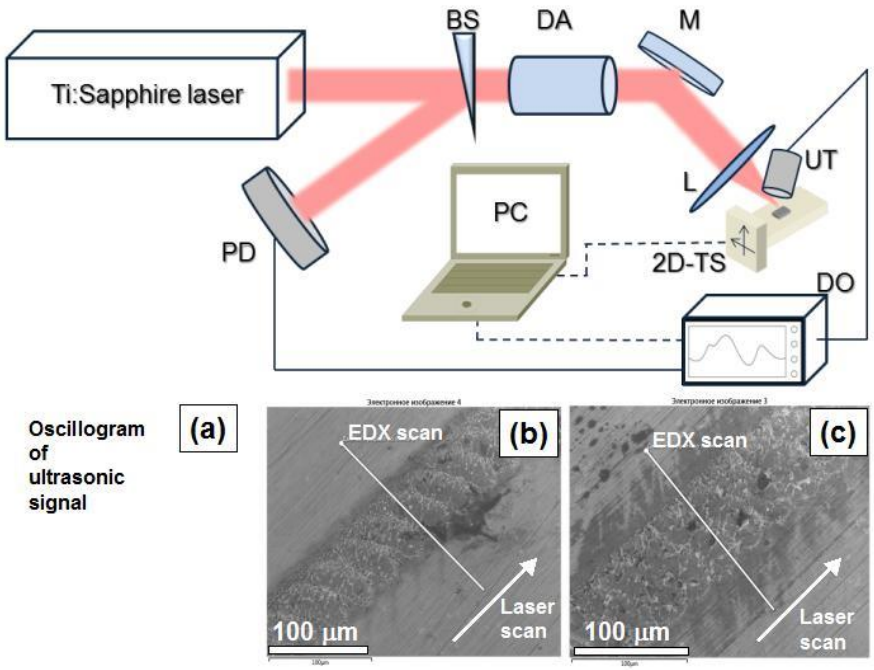

Figure 1. Experimental setup for fs-laser ultrasonic studies and surface peening. Insets: (a) characteristic ultrasonic transient with its basic characteristics – transit time T_{TR}, FWHM time T_W and pressure amplitude P_{TR}, (b,c) top-view SEM image of the AA5083 Al-alloy surface ablated in the scanning mode by single fs-laser pulses at the peak fluences $F_0 \approx 1.3$ (left image, overlap ≤30%) and 4.1 (right image overlap ≤60%) J/cm^2 with the corresponding EDX-scan positions.

3. Results and discussion

3.1. Surface ablation of AA5083 Al-alloy: SEM and ultrasonic studies

SEM inspection of the single-shot ablated Al-alloy surfaces reveals distinct patterns of threshold-like ablative modification (craters), emerging within the focal spots for local fluences $F \geq 0.4$ J/cm^2 (Fig.1b,c). The ablated regions exhibit central micro-scale ablative roughness without pronounced cratering and lateral surface decontamination/oxide removal (dark peripheral areas on the SEM images in Fig.1). These general observations are in agreement with the previous detailed single-shot fs-laser surface ablation studies on pure bulk Al samples, demonstrated distinct surface cratering above the sub-critical spallation and near-critical phase explosion thresholds, $F_{SP} \approx 0.7$ J/cm^2 and $F_{EXP} \approx 1.4$ J/cm^2 [7,22-23], respectively, with sub-critical surface boiling starting below F_{SP} in the form of sub-micron boiling surface pits at $F_B \approx 0.7$ J/cm^2 [23].

Similarly, the acquired ultrasonic transients exhibit a monotonous fluence-dependent decrease of their transit times T_{TR} and increase of their amplitudes P_{TR}, which become strongly pronounced, starting from $F_P \approx 1.5$ J/cm^2 (Fig.2). This is consistent with our previous observation of strong ablative pressure rise during surface ablation of Al for fluences $\geq F_{EXP} \approx 1.3$ J/cm^2 [7]. Likewise, in this work the calculated initial ablative plume pressures P_{ABL} increase almost linearly versus F_0 above the threshold F_{EXP} in the range of 350-3000 GPa, indicating the corresponding linearly increasing deposited volume energy density in the sample and resulting Mbar-strong shock waves in agreement with our previous experimental

measurements and other calculations (see bibliography in [7,11,19] and discussion below). Below the threshold F_{EXP}, the calculated magnitudes P_{ABL} is at sub-GPa level, corresponding to typical critical pressures for normally solid substances (~0.1-1 GPa) [24]. Moreover, there is a strong correlation in double logarithmic coordinates between the experimental curve $P_{TR}(F_0)$ and the curve $P_{ABL}(F_0)$, calculated on the basis of the independent dataset $T_{TR}(F_0)$, indicating the non-linear, self-similar SW propagation in air from the ablation source toward the transducer.

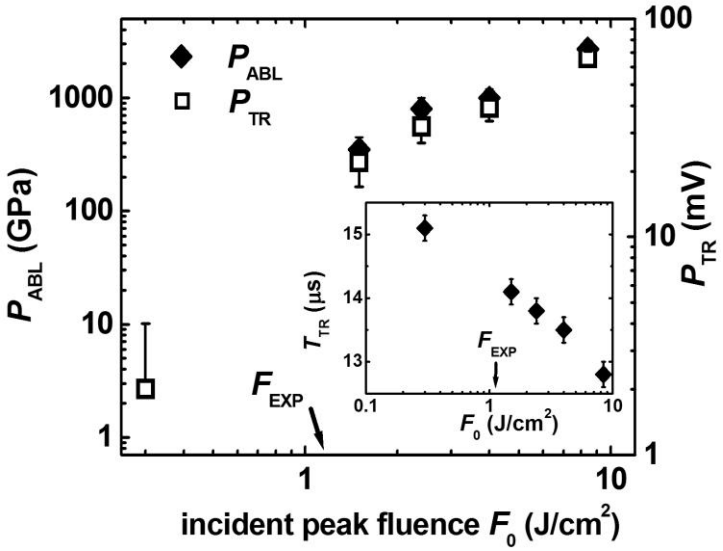

Figure 2. Fluence dependences of ablative pressure P_{ABL} (dark rhombs) and ultrasonic amplitude P_{TR} (light squares). Inset: variation of transit time magnitude T_{TR} versus F_0 (dark rhombs).

Such dramatic enhancement of ablative pressure in Al was previously predicted to yield from near- or supercritical phase explosion [25-27], resulting in explosive hydrodynamic expansion of a vapor-droplet mixture and multi-GPa recoil pressures on the ablated target. The previously simulated strong, though still sonic waves [26,27] with peak pressure $P \approx 20$ GPa < G (where $G = \rho_l C_l^2 \approx 60$ GPa is the bulk modulus in molten Al for its mass density ρ_l close, not strongly differing from the solid one ≈ 2.7 g/cm^3 [24] and the longitudinal sound speed $C_l \approx 4.7$ km/s [24]) were predicted to propagate ~100 nm prior their complete dissipation [27], in qualitative agreement with experimental measurements [10].

3.2 Micro-hardness, residual stresses and crystallites in the peened AA5083 Al-alloy surface layer

In this work, the 1cm×1cm square surface region of the AA5083 Al-alloy peened at the peak fluence $F_0 \approx 5$ J/cm^2 exhibits, on average over 10 imprints, microhardness value of 1.36±0.12 GPa (Fig.3), which is increased almost by 50% regarding the hardness of its untreated reference surface, ≈0.94 GPa. This result is important advance in increasing surface hardness of Al-alloys, which were peened before to attain the typical increase in hardness by 20% upon multi-shot fs-laser [28] and ns-laser exposures (see the review [29] for Al and other materials). Therefore, it is the Mbar-level of the ablative recoil pressure amplitudes that is responsible for the strongly increased surface hardness of the AA5083 Al-alloy peened by the ultrashort laser pulses in this study.

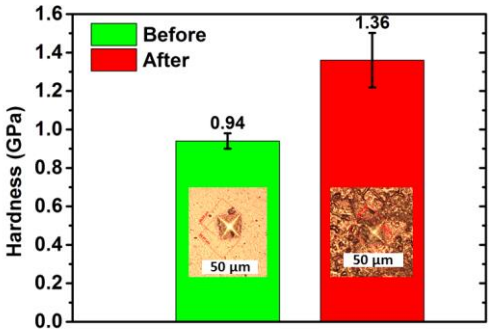

Figure 3. Variation of microhardness for the AA5083 Al-alloy surface spot peened at the peak fluence F_0 ≈ 5 J/cm^2 and for its untreated reference surface spot, with the insets showing the typical imprints of the indenter.

These observations are supported by our XRD measurements, demonstrating considerable sub-surface residual tensile strains (stresses), as a compensation for the near-surface compressive stresses, increasing the surface hardness [30]. Specifically, our comparative analysis of angular (2θ) dependences of x-ray diffraction intensity for the peened and untreated surface spots of the AA5083 Al-alloy shows in the former case the minor, permanent and angular-dependent displacement Δθ of x-ray diffraction peaks over the entire angular range toward lower angles (Fig.4,5). According to the Bragg's law, such negative peak displacements correspond to extended spacings between crystallographic planes, i.e., tensile strains $\xi \approx -\frac{\cos\theta}{\sin^2\theta}\Delta\theta \sim 10^{-4}\text{-}10^{-3}$ rad, with the corresponding main components of the tensile stress $\sigma_1 + \sigma_2 = -(E/\mu)\xi \sim 0.1$ GPa for $\Delta\theta \sim 10^{-4}\text{-}10^{-3}$ rad (Fig.5), where the Young modulus $E \approx 70$ GPa and the Poisson coefficient $\mu \approx 0.31$ for pure Al [24].

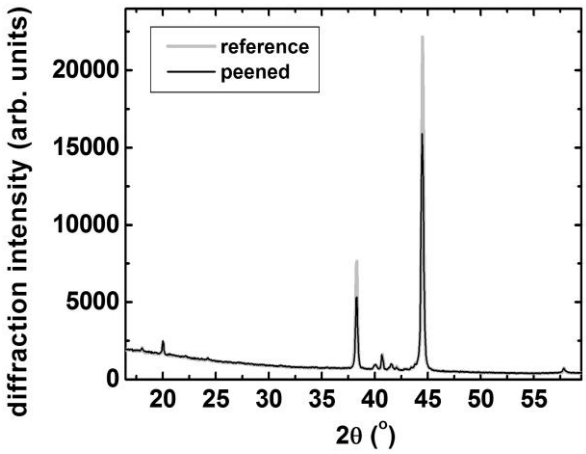

Figure 4. X-ray diffraction spectra from the untreated (reference) and laser-peened surface spots of the AA5083 Al-alloy (see the text for details).

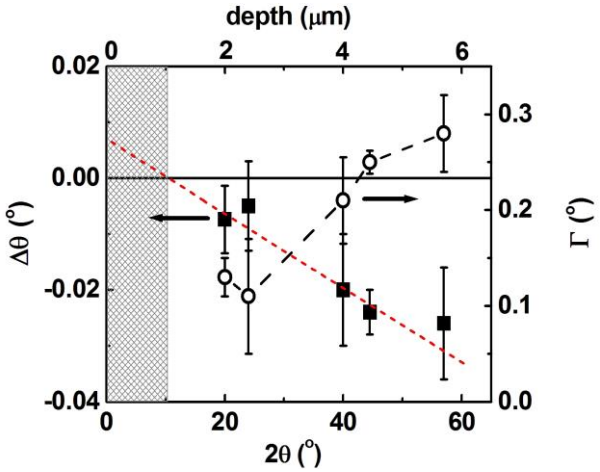

Figure 5. Angular and in-depth dependences of displacement Δθ and width Γ, respectively, of the different x-ray diffraction peaks in Figure 4 for the laser-peened AA5083 Al-alloy surface spot. The dashed line shows the linear approximation of the former curve and its extrapolation to the surface.

Unfortunately, since different angles θ represent probing crystalline structure at variable depths in the non-powder AA5083 Al-alloy sample [9], common Williamson-Hall plot analysis is not applicable in this case owing to the spatially inhomogeneous stresses in the peened material. Meanwhile, more detailed analysis indicates that the compensating sub-surface tensile stresses monotonously decrease toward the peened surface both in terms of peak shifts Δθ and stress-induced broadening Γ (Fig.5), implying, upon rough extrapolation of the former curve Δθ(2θ) to the surface in Figure 5, compressive residual near-surface stresses ~0.1 GPa. More exactly, the sub-GPa-level tensile residual stresses in the multi-micron thick sub-surface layer are supposed to compensate sub-GPa compressive residual stresses in the much thinner (≈1-micron thick, Fig.5) near-surface layer, in agreement with our micro-hardness measurements. According to Huber and Heerens [33] uniaxial compressive residual stresses of 100 MPa cause an increase in microhardness by around 3 %. Therefore, the measured surface microhardness increase by nearly 50 % should be attributed to significant severe surface damages as well as deformations in the microstructure. The surface microstructural changes are also known for conventional shot peening process [34]. Contrary to the femtosecond peening, generation of deep compressive residual stress profiles without noticeable surface damages is still possible for nanosecond laser shock peening process [35].

Николай, можете написать здесь что-то про механику этого сплава???

3.3 *Chemical modification within the single-shot peened AA5083 Al-alloy surface layer*

Chemical EDX microanalysis of the AA5083Al-alloy surface spots single-shot peened at the peak fluences $F_0 \approx 1.5$ and 5 J/cm^2, was performed in this work at variable electron energies K to provide qualitative and quantitative comparison of surface-to-bulk chemical surface modification of the material. Here, higher electron energies $K > 10$ keV were considered as penetrating to and inducing characteristic

X-ray fluorescence from micrometer depths inside the material [31], while the lower energies probed sub-micron depths.

The measured relative contents C_i of the main chemical components demonstrate their considerable variation for both these ablation regimes (Fig.6), with the except for Mg with its content C_{Mg} persisting at the same level of 4.4% irrespectively of K, while the other minor elements – Fe, Si, Zn, Cu, Cr, Ti – keep the same overall content < 0.4%. In particular, comparing to the asymptotic (bulk) content $C_{Al} \approx 94\%$ in Fig.6, it becomes significantly reduced – till 70% or less – in favor of incoming oxygen (O, $C_O \leq 10$ %) and carbon (C, $C_C \approx$ 15-20%), indicating significant post-ablative oxidation and organic contamination of the peened hot surfaces [32], as justified by their almost same contents in both the ablation regimes.

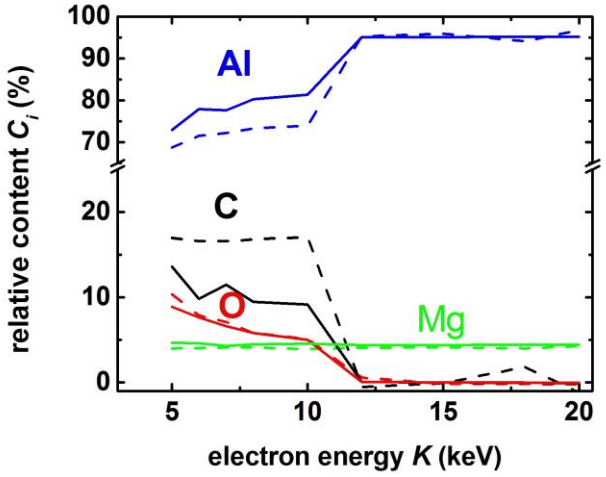

Figure 6. Relative content C_i of the main chemical components on the AA5083 Al-alloy surface peened at the peak fluences $F_0 \approx 1.5$ (dashed curves) and 5 (continuous curves) J/cm^2, versus EDX electron energy K (the initial main contents are shown by the vertical arrows for the reference).

More elaborate interpretation of the EDX data presented in Fig.7 in terms of K-dependent electron penetration depth δ [31] enables to clarify the obtained surface chemical modification. Specifically, the observed carbon and oxygen contents at high K-values are not supported by their real bulk presence, but reflect their surface contribution, asymptotically decreasing at higher K. Hence, in the spatial (depth) profiles their arte-fact asymptotic values of ≈5% (O) and ≈10-16% (C) can be subtracted and added to the main component (Al), restoring its bulk magnitude ≈94%. In contrast, the low-K content values appear to be more relevant, representing the very surface oxidation and carbonization of the material. The derived spatial elemental profiles (Fig.7), in order to reduce the surface arte-fact influence, were extrapolated to the lowest resonance energy of Al, 2 keV, exhibiting the realistic contents $C_C \approx$ 15-20% and $C_O \approx$ 15-20% in the 100-nanometer thick surface layer, respectively.

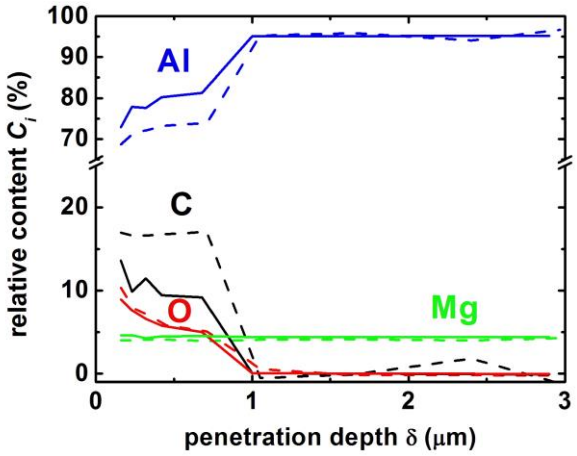

Figure 7. Spatial profiles of relative content C_i of the main chemical components on the AA5083 Al-alloy surface versus *K*-dependent electron penetration depth δ (the asymptotic bulk values C_i show their initial surface contents).

Surprisingly, the sub-micron thickness of the Al-alloy surface layer chemically modified by single fs-laser pulse, according to Fig.7, is not an arte-fact, but represent the strong microscale roughness of the layer. This is in agreement with previous observations of micro-porous, strongly oxidized and carbonized Al surface for the high-fluence fs-laser ablation regime [32] and may strongly affect fs-laser induced micro-hardness of fs-laser peened Al-alloy surfaces, requiring their etching post-processing. For example, recently, 2024 aluminum alloy peened by multi-shot high-fluence fs-laser pulses, demonstrated rather low, but purely compressive residual stresses and enhanced microhardness at multi-micron sub-surface depths [28], but simultaneously the strong reduction of the latter characteristic in the 1-2 micron-thick micro-porous surface layer, supported by TEM analysis of its defective microstructure with micro-voids and dislocations.

4. Conclusions

Single-shot high-fluence femtosecond laser peening of AA5083 Al-alloy surface was used in this study to achieve its increased micro-scale mechanical hardness and to investigate underlying structural and chemical processes. Femtosecond laser surface peening was performed under experimental conditions of SEM-visualized intense ablation of the alloy surface, with corresponding ablative recoil pressures controlled remotely via acquisition of air-borne pressure waves from the ablative plumes. These measurements revealed strong rise of ablative recoil pressures to a Mbar-level above the near-critical phase explosion threshold and their following almost linear fluence-dependent increase in supercritical ablative plumes, hydrodynamically expanding on a nanosecond timescale. The high-fluence single-shot peening yields in AA5083 Al-alloy surface hardness, increased by nearly 50% – from 0.9 till 1.4 GPa. X-ray diffraction characterization of the peened sample revealed sub-GPa-level residual compressive stresses in the micron-thick surface layer, responsible for its increased hardness, with the compensating residual sub-GPa-level tensile stresses buried at multi-micron depths underneath. The single-shot ablative peening does not result in prominent variation of main chemical components (Al, Mg) on the alloy

surface, with the except for its considerable post-ablative oxidation and carbonization via interaction with the ambient atmosphere.

Acknowledgements

This work was supported by the Government of the Russian Federation (Grant 074-U01) for ITMO University.

References

1. F. Korte, J. Serbin, J. Koch, A. Egbert, C. Fallnich, A. Ostendorf, and B.N. Chichkov, Towards nanostructuring with femtosecond laser pulses, Applied Physics A **77**, 229-235 (2003).

2. A.A. Ionin, S.I. Kudryashov, S.V. Makarov, A.A. Rudenko, L.V. Seleznev, D.V. Sinitsyn, E.V. Golosov, Y.R. Kolobov, and A.E. Ligachev, Beam spatial profile effect on femtosecond laser surface structuring of titanium in scanning regime, Applied Surface Science **284**, 634-637 (2013).

3. C. Wu, M.S. Christensen, J.M. Savolainen, P. Balling, and L.V. Zhigilei, Generation of subsurface voids and a nanocrystalline surface layer in femtosecond laser irradiation of a single-crystal Ag target, Physical Review B **91**, 035413 (2015).

4. D. Bauerle, *Laser Processing and Chemistry*, Springer, Berlin, 2011.

5. R. Evans, A. D. Badger, F. Falliès, M. Mahdieh, T. A. Hall, P. Audebert, J.-P. Geindre, J.-C. Gauthier, A. Mysyrowicz, G. Grillon, and A. Antonetti, Time-and space-resolved optical probing of femtosecond-laser-driven shock waves in aluminum, Physical Review Letters **77**, 3359-3362 (1996).

6. T. Sano, H. Mori, E. Ohmura, and I. Miyamoto, Femtosecond laser quenching of the ε phase of iron, Applied Physics Letters **83**, 3498-3500 (2003).

7. A.A. Ionin, S.I. Kudryashov, S.V. Makarov, L.V. Seleznev, and D.V. Sinitsyn, Generation and detection of superstrong shock waves during ablation of an aluminum surface by intense femtosecond laser pulses, JETP Letters **94**, 34-38 (2011).

8. E.I. Ageev, V.P. Veiko, S.I. Kudryashov, A.A. Petrov, and A.A. Samokhvalov, Contact and non-contact ultrasonic diagnostics of shock waves driven by single-shot femtosecond laser ablation of titanium, JETP Letters **120**, 693-696 (2015).

9. Yu. R. Kolobov, T.N. Vershinina, M.V. Zhidkov, E.V. Golosov, A.A. Ionin, S.I. Kudryashov, S.V. Makarov, L.V. Seleznev, D.V. Sinitsyn, and A.E. Ligachev, Structural transformation and residual stresses in surface layers of α+β titanium alloys nanotextured by intense femtosecond laser pulses, Applied Physics A **119**, 241-247 (2014).

10. S.I. Ashitkov, P.S. Komarov, E.V. Struleva, M.B. Agranat, and G.I. Kanel', Mechanical and optical properties of vanadium under shock picosecond loads, JETP Letters **101**, 276-281 (2015).

11. E.I. Ageev, S.I. Kudryashov, N.V. Nikonorov, R.K. Nuryev, A.A. Petrov, A.A. Samokhvalov, and V.P. Veiko, Non-contact ultrasonic acquisition of femtosecond laser-driven ablative Mbar-level shock waves on Ti alloy surface, Applied Physics Letters **108**, 084106 (2016).

12. D. Lee, and E. Kannatey-Asibu, Jr., Experimental investigation of laser shock peening using femtosecond laser pulses, J. Laser Applications **23**, 022004 (2011).

13. Y. Ye, Y. Feng, Z. Lian, and Y. Hua, Plastic deformation mechanism of polycrystalline copper foil shocked with femtosecond laser, Applied Surface Science **309**, 240-249 (2014).

14. Y. Ye, Y. Feng, Z. Lian, and Y. Hua, Mold-free fs laser shock micro forming and its plastic deformation mechanism, Optical and Laser Engineering **67**, 74-82 (2015).

15. H. Nakano, S. Miyauti, N. Butani, T. Shibayanagi, M. Tsukamoto, and N. Abe, Femtosecond laser peening of stainless steel, J. Nano- and Microengineering **4**, 35-38 (2009).

16. R. Fabbro, P. Peyre, L. Berthe, and X. Scherpereel, Physics and applications of laser-shock processing, Journal of laser applications, J. Laser Applications **10**, 265-279 (1998).

17. B. Wu, S. Tao, and S. Lei, Numerical modeling of laser shock peening with femtosecond laser pulses and comparisons to experiments, Applied Surface Science **256**, 4376-4382 (2010).

18. G.I. Kanel', V.E. Fortov, and S.V. Razorenov, Shock waves in condensed-state physics, Physics-Uspekhi **50**, 771-791 (2007).

19. N. Zhang, X. Zhu, J. Yang, X. Wang, and M. Wang, Time-resolved shadowgraphs of material ejection in intense femtosecond laser ablation of aluminum, Physical Review Letters **99**, 167602 (2007).

20. E.I. Ageev, V.Yu. Bychenkov, A.A. Ionin, S.I. Kudryashov, A.A. Petrov, A.A. Samokhvalov, and V.P. Veiko, Double-pulse femtosecond laser peening of aluminum alloy AA5038: effect of inter-pulse delay on transient optical plume emission and final surface micro-hardness, Applied Physics Letters **109**, 211902 (2016).

21. Ya.B. Zel'dovich, and Yu.P. Raizer, *Physics of Shock Waves and High-Temperature Hydrodynamic Phenomena*, Dover, New York, 2002.

22. M.A. Gubko, W. Husinsky, A.A. Ionin, S.I. Kudryashov, S.V. Makarov, C. Nathala, A.A. Rudenko, L.V. Seleznev, D.V. Sinitsyn, and I.V. Treshin, Enhancement of Photoemission of Ultrafast Electrons from a Femtosecond Laser-Induced Array of Metallic Nanotips, Laser Physics Letters **11**, 065301 (2014).

23. A.A. Ionin, S.I. Kudryashov, S.V. Makarov, Alexey O. Levchenko, Andrey A. Rudenko, Irina N. Saraeva, Dmitry A. Zayarny, C.R. Nathala, and W. Husinsky, Nanoscale boiling in sub-threshold surface damage and threshold-like surface spallation of bulk aluminum and gold by single femtosecond laser pulses, Laser Physics Letters **13**, 025603 (2016).

24. I.S. Grigor'ev, and E.Z. Meylikhov, *Physical Quantities* (Energoatomizdat, Moscow, 1991).

25. S. Sonntag, C. TrichetParedes, J. Roth, and H.-R. Trebin, Molecular dynamics simulations of cluster distribution from femtosecond laser ablation in aluminum, Applied Physics A **104**, 559-565 (2011).

26. C.Wu, and L.V. Zhigilei, Microscopic mechanisms of laser spallation and ablation of metal targets from large-scale molecular dynamics simulations, Applied Physics A **114**, 11-32 (2014).

27. D.S. Ivanov, V.P. Lipp, V.P. Veiko, E. Yakovlev, B. Rethfeld, and M. E. Garcia, Molecular dynamics study of the short laser pulse ablation: quality and efficiency in production, Applied Physics A **117**, 2133-2141 (2014).

28. T. Sano, T. Eimura, R. Kashiwabara, T. Matsuda, Y. Isshiki, A. Hirose, S. Tsutsumi, K. Arakawa, T. Hashimoto, K. Masaki, and Y. Sano, Femtosecond laser peening of 2024 aluminum alloy without a sacrificial overlay under atmospheric conditions, J. Laser Applications **29**, 012005 (2017).

29. C.S. Montross, T. Wei, L. Ye, G. Clark, and Y.-W. Mai, Laser shock processing and its effects on microstructure and properties of metal alloys: a review, International Journal of Fatigue **24**, 1021–1036 (2002).

30. Y. Zhang, W. H. Wang, and A. L. Greer, Making metallic glasses plastic by control of residual stress, Nature materials **5**, 857-860 (2006).

31. K. Kanaya, and S. Okayama, Penetration and energy-loss theory of electrons in solid targets, J. Physics D: Applied Physics **5**, 43-58 (1972).

32. X. Li, C. Yuan, H. Yang, J. Li, W. Huang, D. Tanga, and Q. Xu, Morphology and composition on Al surface irradiated by femtosecond laser pulses, Applied Surface Science **256,** 4344–4349 (2010).

33. N. Huber, J. Heerens, On the effect of a general residual stress state on indentation and hardness testing, Acta Materialia **56**, 6205-6213 (2008).

34. A. Gariépy, F. Bridier, M. Hoseini, P. Bocher, C. Perron, M. Lévesque, Experimental and numerical investigation of material heterogeneity in shot peened aluminium alloy AA2024-T351, Surface & Coatings Technology **219**, 15-30 (2013).

35. N. Kashaev, V. Ventzke, M. Horstmann, S. Chupakhin, S. Riekehr, R. Falck, E. Maawad, P. Staron, N. Schell, N. Huber, Effects of laser shock peening on the microstructure and fatigue crack propagation behaviour of thin AA2024 specimens, International Journal of Fatigue, in press.